Computational investigation of intramolecular reorganization energy in diketopyrrolopyrrole (DPP) derivatives

Şule ATAHAN EVRENK

Faculty of Medicine, TOBB University of Economy and Technology, Ankara, Turkey

Computational investigation of intramolecular reorganization energy in diketopyrrolopyrrole (DPP) derivatives

Şule ATAHAN EVRENK

Faculty of Medicine, TOBB University of Economy and Technology, Ankara, Turkey

Correspondence: satahanevrenk@etu.edu.tr

Abstract: Intramolecular reorganization energy (RE) of molecules derived from the diketopyrrolopyrrole (DPP) unit has been studied using the B3LYP/6-31G(d,p) theory. It was found that the replacement of the oxygen atoms with sulfur in the DPP unit led to a smaller RE for both the hole and electron transfer processes. One disadvantage of the sulfur replacement is the twist of the conjugated backbone which might impair the π–π interactions in the solid state. The RE calculated from the adiabatic potential energy surfaces and that derived from the normal mode analysis agreed well for both the systems. Electronic structure data showed that the replacement of oxygen atoms with sulfur in the DPP unit might lead to the development of ambipolar compounds with low RE.

Key words: Diketopyrrolopyrrole, dithiopyrrolopyrrole, reorganization energy, charge transfer

1. Introduction

-- Figure 1 --

The electron-deficient diketopyrrolopyrrole (DPP) unit (Figure 1) has been extensively used to build organic semiconductors (OSCs) for transistors, [1–3] organic photovoltaics (OPVs), [2,4–6] and light emitting diodes. It has also been utilized for building compounds for imaging purposes. [7] Both the highest occupied molecular orbital (HOMO) and the lowest

unoccupied molecular orbital (LUMO) of DPP are low-lying. Moreover, strong π–π interactions among the DPP units in the polymers facilitate aggregation and improve the device performance. Therefore, the DPP unit has emerged as a versatile building block for small band gap OPV compounds as well as organic field-effect transistors (OFETs) with ambipolarity. [8]

Charge mobility plays a crucial role in the device performance, which is important for all electronics applications. Reorganization energy (RE) is one of the most important charge transport parameters that strongly influences charge mobility. It refers to the relaxation energy for the nuclei to adapt to the charge transfer process. The smaller the RE, the higher is the charge transfer rate. For example, in the non-adiabatic Marcus charge transfer theory, the rate of charge transfer decreases exponentially with the increasing RE. [9]

In molecular van der Waals solids, an approximate RE value can be calculated based on the assumption that the intramolecular electron-vibronic coupling is the largest contributor to the RE. [10] The external contribution to the RE was found to be much smaller than the intramolecular contribution. [11] Moreover, the intramolecular RE has been successfully used for the theoretical characterization of OSCs and screening of molecules to identify the potential for high performance. [10,12,13] Thus, in this study, we have focused on the intramolecular RE, and henceforth, RE refers in particular to the intramolecular RE.

Understanding the structural factors that affect the magnitude of the RE is helpful for improving OSC designs. Consequently, a lot of effort has been dedicated to the investigation of the relationship between the molecular structure and RE. The effect of a

particular conjugated backbone structure [14,15] and the substitutions, [16] in addition to geometrical parameters such as the size, length, and linearity of the conjugated backbone have been previously investigated. [17] In OSCs, the substitutions were usually employed to engineer the carrier type and crystal morphologies, and also to control the solution processability. Most substitutions such as fluorination, chlorination, and alkoxy substitutions, however, increase the RE. [18] Therefore, it is of interest to find design strategies that reduce the RE in OSCs.

-- Figure 2 --

Among the studies of the RE with the molecular structure, the ones which present a detailed study of the electron-vibration coupling in terms of the individual contributions from the particular couplings of vibrational modes to the electronic motion is of great value. They provide a quantitative basis for the identification of the structure-property relationships. [16,19,20] In this work, first we present such an analysis of the RE for the molecular structures shown in Figure 2. In the first molecule (**1**), the two sides of the DPP unit are flanked with two thiophene rings. Molecule **2** is the sulfur analogue of molecule **1**, where the oxygen atoms are replaced with sulfur atoms. We studied molecule **2** to test the hypothesis that hindering the short axis stretching motion might reduce the strong coupling seen in the case of molecule **1** and consequently reduce the magnitude of the RE. Therefore, we performed a detailed analysis of the couplings of the electronic motion with the particular vibrational modes in molecules **1** and **2** for both the hole- and electron-transfer processes. To test the hypothesis in a larger library, we extend the molecular library to six molecules obtained by

flanking one of the ends of molecule 1 and 2 with either one of the heterocycles: thiophene, furan or selenophene.

Previous research on the dithiopyrrolopyrrole (DTPP) unit has been rather limited. To the best of our knowledge, there are only two previous reports. [21,22] One study investigates the structural isomers of the dithiopyrrolopyrrole unit [19] and the other demonstrates that the unit can be used as an acceptor in low band gap donor-acceptor polymers produced for OPV and near-IR photo detector applications. [20] At present, there are no studies analyzing the RE for molecule **2**. The RE for the derivatives of molecule **1**, obtained by the addition of various thiophene groups to **1**, has been reported. [23] Makarova et al studied another oligomer derived from molecule **1** by flanking the both ends with thiophene rings. [24] None of these works however include a detailed analysis of the RE to examine the couplings from particular vibrational modes to the charge transfer process.

In the following, we summarized the computational methodology and focused on the detailed comparison of the RE for molecules **1** and **2**. The RE values calculated for the extended set show that the substitution lowers the RE in molecules derived from **1** and **2** as well. This work presents a structural variation that can lower the RE, and thus aims to contribute to the improvement of the computational strategies in the design of OSC materials. It is worth noting that several factors affect the charge mobility as well, and it is not reasonable to conclude that the molecular variation discussed here is going to lead to a certain expected experimental device performance. It is our objective to simply determine whether further experimental study can be potentially beneficial.

2. Computational methods

-- Figure 3--

There are various approaches to calculating the RE that have been reported in literature. Assuming a gas-phase self-exchange type of a charge transfer reaction such as $\boldsymbol{M_1} + \boldsymbol{M_2}^{+/-} \rightarrow \boldsymbol{M_1}^{+/-} + \boldsymbol{M_2}$, the RE can be calculated according to a four-point scheme from the adiabatic potential energy surfaces of the neutral and ionic states of the molecule. [19,25] Figure 3 illustrates this scheme for the hole transfer process. This adiabatic scheme captures the relaxation energies during the charge transfer from a neutral molecule to a neighboring ion of the same molecule. The computation involves two geometry optimizations and four single-point calculations and the RE is derived from the total energy differences.

This total energy difference approach does not provide information about the RE contributions from the coupling of specific vibrational modes to the electronic motion. The contribution from a particular vibration-electronic coupling to the RE can be determined by using a decomposition method previously outlined by Reimers. [26] In this method, first the dimensionless projection of the coordinate displacements onto the normal modes of the neutral or ionic state are calculated. This is done according to the following equation:

$$\boldsymbol{\delta_1} = \mathbf{I_1^{-1}} \boldsymbol{C_1^T} \boldsymbol{m^{\frac{1}{2}}} (\mathbf{x_2^0} - \mathbf{x_1^0})$$

Here $\mathbf{I}_1$ refers to the zero-point lengths of the normal modes and is defined as $I_{1ii} = \left(\frac{\hbar}{2\pi\nu_{1i}}\right)^{1/2}$ for the neutral ground state, where ν_{1i} is the *i*th vibrational frequency. $\boldsymbol{C_1}$ is a $3n \times n_v$ matrix including the normal mode coordinates (*n* atoms have $n_v = 3n - 6$ normal

coordinates); $\boldsymbol{m}$ is a $3n \times 3n$ diagonal matrix which has the corresponding atomic masses for the Cartesian coordinates; and $\mathbf{x_1^0}$ and $\mathbf{x_2^0}$ are the Cartesian coordinates for the optimized neutral and ion geometries, respectively. Note that the normal modes are the eigenvectors of the mass-weighted Hessian matrix. If the normal modes were not mass-weighted, such as in the case of the output from the Q-Chem frequency calculation, the normal vectors are multiplied with a correction factor such as $C_{1i} \times \sqrt{m_j}/\sqrt{\mu_{1i}}$, where μ_i is the reduced mass for the particular normal mode *i*, and m_j is the mass of the *j*th atom.

Thus, δ_{1i} is a unitless projection of the change in the Cartesian coordinates onto the normal coordinates of the molecule in the neutral state. The same relationship can then be used to obtain δ_{2i}, which is the projection of the same vector onto the normal coordinates of the molecule in the ionic state. The relationship of δ with the well-known Huang-Rhys factor is $S = \frac{\delta^2}{2}$.[9]

The dimensionless projection δ_{1i}, is then used to calculate the contribution of each normal mode of the neutral geometry to the RE as $\lambda_{1i} = \frac{h}{2}\nu_{1i}\delta_{1i}^2$. The total RE for the neutral mode projection is obtained as $\lambda_1 = \sum_{i=1}^{n} \lambda_{1i}$. The same sequence can be repeated for the ionic state and the contributions to total RE are calculated by the projection of the Cartesian displacements onto the normal modes of the ionic state as $\lambda_2 = \sum_{i=1}^{n} \lambda_{2i}$, where $\lambda_{2i} = \frac{h}{2}\nu_{2i}\delta_{2i}^2$. Finally, the total RE is obtained by a simple sum of the neutral and ionic contributions as $\lambda = \lambda_1 + \lambda_2$.

131 The initial geometries were obtained with the ChemAxon geometry plugin. [27] The
132 geometries were optimized with the B3LYP/6-31G(d,p) density functional theory, [28–32]
133 except for the anion geometries, where the basis set (6-31G+(d,p)) with diffuse functions
134 was used. The tight convergence thresholds were held throughout. The true minima were
135 confirmed by the absence of the negative vibrational frequencies. It was observed that the
136 spin contamination was always less than 4% for the ionic states. All electronic structure
137 calculations were performed using Q-Chem 4.2. [33] The normal mode analysis of the RE
138 was performed by using an in-house Python code.

139 **3. Results and discussion**

140 **3.1. Geometry**

141 - Figure 4--

142 The optimized geometries for the lowest energy conformers of the molecules are shown in
143 Figure 4. A flat backbone for molecule **1** can be observed regardless of whether symmetry
144 has been imposed or not. This is also true for both the cation and anion states. In contrast,
145 the large sulfur atoms in **2** cause the backbone to twist, resulting in dihedral angles along
146 the N–C–C–S atoms as 27.5°, 25.8°, and 27.6° for the neutral, cation, and anion
147 geometries, respectively. Therefore, the presence of sulfur atoms instead of oxygen in the
148 DPP unit might adversely influence the π–π interactions in the solid state.

149 -- Figure 5--

150 Bond length alternation, calculated as $\boldsymbol{BLA = R_2 - R_1}$, where $\boldsymbol{R_1}$ and $\boldsymbol{R_2}$ refer to bond
151 lengths of two consecutive bonds along the conjugation length, provides an insight into the
152 relaxation process. Figure 5 illustrates how BLA varies along the conjugation length of the

153 molecules for the neutral, anion, and cation states. The BLA for all of the species are
154 symmetric and the neutral and anion alternations show a trend similar to the conjugation
155 structure shown in Figure 5a. This is also true for molecule **2**. In contrast, the cation BLA
156 distributions have a reverse BLA pattern for the DPP unit, which indicates the switch of the
157 double bond to a position in between the shared carbon atoms of the pyrrole cycles (bond 6
158 in Figure 5a). The same is true for the cationic state of molecule **2** as well. For both
159 molecules, smaller geometric distortions are generally observed upon electron transfer.
160 Therefore, a smaller RE value for electron transfer is expected in comparison to hole
161 transfer from the analysis of the BLA patterns.
162 -- Table 1 --
163 Table 1 presents the electronic structure data and the RE values obtained from the potential
164 energy surfaces and the normal mode analysis for molecules **1** and **2**. The introduction of
165 the sulfur atoms into the DPP unit reduces the frontier orbital energies, and increases the
166 adiabatic ionization potential and electron affinity. The carrier type of an OSC can be
167 correlated with the frontier orbital energy levels. [34,35] The polymers derived from molecule
168 **1** shown ambipolar conductance in the OFETs. Based on the lower HOMO and LUMO
169 values for molecule **2**, a potential for ambipolar mobility of the polymers derived from this
170 unit is expected.
171 In addition to the frontier molecular orbital energy levels of the neutral molecule, we also
172 report the HOMO values for the optimized cation geometry ϵ_{homo}^{c}. A previous study [17]
173 showed that the HOMO energy difference $\epsilon_{homo}^{c} - \epsilon_{homo}$ is a good predictor of the RE [17]
174 for the hole transfer in polyaromatic hydrocarbons. Although this observation is strictly true

for an exact exchange-correlation functional, for the hybrid functional employed here the energy difference is also a good descriptor of the reorganization energy. The difference is 327 and 218 meV for molecules **1** and **2**, respectively, which closely resembles the λ_+ values of 331 and 217 meV obtained from the potential energy surfaces.

The RE for the hole transfer is above average compared to other high-performance OSCs. For example, the RE of hole transfer in pentacene is 98 meV. [36] On the other hand, it was found that the RE for the electron transfer, λ_-, was almost half of that of the hole transfer process. This explains the high electron mobility measurements in these materials [1].

The substitution with sulfur atoms in the DPP unit leads to a 35% decrease in the RE for hole transfer. Albeit more moderate, there is also a decrease (~18%) in the RE for the electron transfer process. Therefore, an improvement in the both the charge transfer rates is expected based on the assumption that the substitution does not change the intermolecular electronic coupling. In the next section, we present the details of the coupling and the reasons for the decrease in the RE upon sulfur substitution.

3.2. Vibronic coupling and molecular orbital shapes

-- Figure 6--

Figure 6 shows the distribution of the relaxation energy over the vibrational frequencies of molecules **1** and **2**. For brevity, only the projections to the normal modes of the neutral ground state, $\boldsymbol{\lambda_1}$, have been included. This is because the contributions $\boldsymbol{\lambda_1}$ and $\boldsymbol{\lambda_2}$ are almost equal and show similar distributions. For example, the hole transfer RE components $\boldsymbol{\lambda_1}$ and $\boldsymbol{\lambda_2}$ for molecule **1** are both 166.6 meV, while they are 115 and 105 meV, respectively, for molecule **2**.

--Figure 7--

-- Figure 8--

The shape of the frontier orbitals and the vibrational normal modes with the highest contributions to the RE are shown in Figure 7 and 8 for molecule **1** and **2**, respectively. The exact numbers of all of the electron-vibration couplings are listed in the Tables 2 and 3. Only those frequencies for which a significant electron-vibration coupling observed, such that any one of the Huang-Rhys parameters $\boldsymbol{S_1^+}$ or $\boldsymbol{S_1^-}$ is greater than 0.001, have been reported.

The analysis of the frontier molecular orbitals together with the Huang-Rhys factors provides a fingerprint for the analysis of structure-relaxation relationships. [20,37,38] The coupling is usually strong for those frequencies for which the normal displacements match the pattern of the particular molecular orbital involved in the charge transfer process. This would be the HOMO for the hole transfer and the LUMO for the electron transfer. [37] In our analysis, the first notable difference observed on comparing the relaxation energies was that molecule **1** had the strongest contribution from the vibrational mode of 504 cm^{-1} for the hole transfer, although this coupling was very small for the electron transfer process (Figure 6a and 6b). The normal coordinates for this mode are shown in Figure 7a. This normal coordinate involves a vertical stretch of the DPP unit in the molecule. As seen in Figure 7a and 7b, the normal coordinates strongly match the HOMO pattern over the DPP unit. The same stretching mode does not show any significant coupling in the case of the electron transfer. This could be rationalized by evaluating the LUMO in Figure 7c. On the other hand, the stronger coupling for the electron transfer process corresponds to the vibrational

mode with the frequency of 1567 cm^{-1} (Figure 7d). This mode involves the stretching vibration along the long-axis of the molecule **1**.

The replacement of the oxygen atom with the heavier sulfur atom dampens the stretching mode over the DPP unit. In turn, this reduces the coupling of the vibrational mode at 491 cm^{-1} and results in a significant reduction in the RE (as seen in Figure 6a and 6c).

The largest contribution to the hole transfer RE in the case of molecule **2** arises from the coupling of the vibrational mode at 1443 cm^{-1}. The normal mode vectors for the vibration at 1443 cm^{-1} are shown in Figure 8d. For electron transfer, the largest contribution is from the mode at 1137 cm^{-1}.

-- Figure 9 --

The Huang-Rhys factors for the two molecules are shown in Figure 9. Since these factors are dimensionless, a stronger Huang-Rhys value in the lower frequency region indicates a small contribution to the RE. Comparing the Huang-Rhys distributions for molecules **1** and **2** for hole transfer (Figure 9a and 9c), it is evident that the strongest coupling in molecule **2** is for the vibrational frequency of 60 cm^{-1}. Moreover, the Huang-Rhys factors for the high frequency vibrations are very small. For electron transfer, the Huang-Rhys values are smaller in magnitude and the stronger couplings correspond to the low frequency modes in both molecules. In general, this lowers the total RE for the electron transfer as compared to the hole transfer process.

3.3. The extended oligomers

-- Figure 10 --

We further illustrate the reduction of the RE with the sulfur substitution in DPP unit by calculating the RE for a series of compounds derived from molecule **1** and **2**. Figure 10 shows the thiophene, furan and selenophene end-capped molecules, labeled to represent the original molecule from which they are derived. The electronic data for the molecules were summarized in Table 4. Figure 11 clearly shows that the compounds derived from molecule **2** have lower RE compared to the molecule **1** derived analogues. The change in the RE with the replacement of the end heterocycle as we go down the periodic table from oxygen to selenium is smaller than the effect of the sulfur substitution in the DPP unit. Moreover, both the HOMO and LUMO energies decreased after substitutions and this shift is much larger than the effect of the addition of the end heterocyles.

4. Conclusion

In this article, we presented a detailed theoretical analysis for the RE of two derivatives of the DPP unit. We demonstrated that the substitution of the oxygen atoms of the DPP unit with sulfur results in a smaller coupling of the vibrational and electronic motions during charge transfer. In all the molecules we studied, we observed a smaller RE for the electron transfer processes as compared to the hole transfer. The molecular orbital levels and the RE values indicated that molecule **2** could be a viable option as an ambipolar material, with the only caveat being its twisted backbone, which might reduce the π–π interactions in the solid state.

Acknowledgements

This research was financially supported by the TÜBİTAK (The Scientific and Technological Research Council of Turkey) BİDEB 2232 Program (Grant No: 114C153) and software support from ChemAxon Ltd.

References

(1) Nielsen, C. B.; Turbiez, M.; McCulloch, I. *Adv. Mater.* **2013**, *25*, 1859–1880.

(2) Li, Y.; Sonar, P.; Murphy, L.; Hong, W. *Energy Environ. Sci.* **2013**, *6*, 1684–1710.

(3) Sonar, P.; Singh, S. P.; Li, Y.; Soh, M. S.; Dodabalapur, A. *Adv. Mater.* **2010**, *22*, 5409–5413.

(4) Ripaud, E.; Demeter, D.; Rousseau, T.; Boucard-Cétol, E.; Allain, M.; Po, R.; Leriche, P.; Roncali, J. *Dye. Pigment.* **2012**, *95*, 126–133.

(5) Qu, S.; Tian, H. *Chem. Commun.* **2012**, *48*, 3039–3051.

(6) Sonar, P.; Ng, G.-M.; Lin, T. T.; Dodabalapur, A.; Chen, Z.-K. *J. Mater. Chem.* **2010**, *20*, 3626–3636.

(7) Grzybowski, M.; Gryko, D. T. *Adv. Opt. Mater.* **2015**, *3*, 280–320.

(8) Tieke, B.; Rabindranath, A. R.; Zhang, K.; Zhu, Y. *Beilstein J. Org. Chem.* **2010**, *6*, 830–845.

(9) Barbara, P. F.; Meyer, T. J.; Ratner, M. A. *J. Phys. Chem.* **1996**, *100*, 13148–13168.

(10) Coropceanu, V.; Cornil, J.; da Silva Filho, D. A.; Olivier, Y.; Silbey, R.; Bredas, J.-L. *Chem. Rev* **2007**, *107*, 926–952.

(11) McMahon, D. P.; Troisi, A. *J. Phys. Chem. Lett.* **2010**, *1*, 941–946.

(12) Sokolov, A. N.; Atahan-Evrenk, S.; Mondal, R.; Akkerman, H. B.; Sánchez-Carrera, R. S.; Granados-Focil, S.; Schrier, J.; Mannsfeld, S. C. B.; Zoombelt, A. P.; Bao, Z.; Aspuru-Guzik, A. *Nat. Commun.* **2011**, *2*, 437.

(13) Schober, C.; Reuter, K.; Oberhofer, H. *J. Phys. Chem. Lett.* **2016**, *7*, 3973–3977.

(14) Chang, Y. C.; Chao, I. *J. Phys. Chem. Lett.* **2010**, *1*, 116–121.

(15) Chen, H. Y.; Chao, I. *ChemPhysChem* **2006**, *7*, 2003–2007.

(16) Geng, H.; Niu, Y.; Peng, Q.; Shuai, Z.; Coropceanu, V.; Bredas, J. L. *J. Chem. Phys.* **2011**, *135*, 104703.

(17) Misra, M.; Andrienko, D.; Faulon, J.; Lilienfeld, O. A. Von. *J. Chem. Theory Comput.* **2011**, *7*, 2549–2555.

(18) Chen, H. Y.; Chao, I. *Chem. Phys. Lett.* **2005**, *401*, 539–545.

(19) Coropceanu, V.; Cornil, J.; da Silva Filho, D. A.; Olivier, Y.; Silbey, R.; Bredas, J.-L. *Chem. Rev.* **2007**, *107*, 926–952.

(20) Coropceanu, V.; Kwon, O.; Wex, B.; Kaafarani, B. R.; Gruhn, N. E.; Durivage, J. C.; Neckers, D. C.; Brédas, J.-L. *Chem. Eur. J.* **2006**, *12*, 2073–2080.

(21) Nourmohammadian, F.; Yavari, I.; Mirhabibi, A. R.; Moradi, S. *Dye. Pigment.* **2005**, *67*, 15–20.

(22) Qian, G.; Qi, J.; Wang, Z. Y. *J. Mater. Chem.* **2012**, *22*, 12867–12873.

(23) Gunther, F.; Gemming, S.; Seifert, G. *J. Phys. Chem. C* **2016**, *120*, 9581–9587.

(24) Makarova, M. V.; Semenov, S. G.; Guskova, O. A. *Int. J. Quantum Chem.* **2016**, *116*, 1459–1466.

(25) Nelsen, S. F.; Blackstock, S. C.; Kim, Y. *J. Am. Chem. Soc.* **1987**, *109*, 677–682.

(26) Reimers, J. R. *J. Chem. Phys.* **2001**, *115*, 9103–9109.

(27) ChemAxon. *Calculator Plugins, Marvin 15.1.5 (http://www.chemaxon.com)*. 2015.

(28) Becke, A. D. *J. Chem. Phys.* **1993**, *98*, 5648–5652.

(29) Lee, C.; Yang, W.; Parr, R. G. *Phys. Rev. B* **1988**, *37*, 785–789.

(30) Hariharan, P. C.; Pople, J. A. *Theor. Chim. Acta* **1973**, *28*, 213–222.

(31) Francl, M. M.; Pietro, W. J.; Hehre, W. J.; Binkley, J. S.; Gordon, M. S.; Defrees, D. J.; Pople, J. A. *J. Chem. Phys.* **1982**, *77*, 3654–3665.

(32) Hehre, W. J.; Ditchfield, R.; Pople, J. A. *J. Chem. Phys.* **1972**, *56*, 2257–2261.

(33) Shao, Y.; Gan, Z.; Epifanovsky, E.; Gilbert, A. T. B.; Wormit, M.; Kussmann, J.; Lange, A. W.; Behn, A.; Deng, J.; Feng, X.; Ghosh, D.; Goldey, M.; Horn, P. R.; Jacobson, L. D.; Kaliman, I.; Khaliullin, R. Z.; Kuś, T.; Landau, A.; Liu, J.; Proynov, E. I.; Rhee, Y. M.; Richard, R. M.; Rohrdanz, M. A.; Steele, R. P.; Sundstrom, E. J.; III, H. L. W.; Zimmerman, P. M.; Zuev, D.; Albrecht, B.; Alguire, E.; Austin, B.; Beran, G. J. O.; Bernard, Y. A.; Berquist, E.; Brandhorst, K.; Bravaya, K. B.; Brown, S. T.; Casanova, D.; Chang, C.-M.; Chen, Y.; Chien, S. H.; Closser, K. D.; Crittenden, D. L.; Diedenhofen, M.; Jr., R. A. D.; Do, H.; Dutoi, A. D.; Edgar, R. G.; Fatehi, S.; Fusti-Molnar, L.; Ghysels, A.; Golubeva-Zadorozhnaya, A.; Gomes, J.; Hanson-Heine, M. W. D.; Harbach, P. H. P.; Hauser, A. W.; Hohenstein, E. G.; Holden, Z. C.; Jagau, T.-C.; Ji, H.; Kaduk, B.; Khistyaev, K.; Kim, J.; Kim, J.; King, R. A.; Klunzinger, P.; Kosenkov, D.; Kowalczyk, T.; Krauter, C. M.; Lao, K. U.; Laurent, A. D.; Lawler, K. V; Levchenko, S. V; Lin, C. Y.; Liu, F.; Livshits, E.; Lochan, R. C.; Luenser, A.; Manohar, P.; Manzer, S. F.; Mao, S.-P.; Mardirossian, N.; Marenich, A. V; Maurer, S. A.; Mayhall, N. J.; Neuscamman, E.; Oana, C. M.; Olivares-Amaya, R.; O'Neill, D. P.; Parkhill, J. A.; Perrine, T. M.; Peverati, R.; Prociuk, A.; Rehn, D. R.; Rosta, E.; Russ, N. J.; Sharada, S. M.; Sharma, S.; Small, D. W.; Sodt, A.; Stein, T.; Stück, D.; Su, Y.-C.; Thom, A. J. W.; Tsuchimochi, T.; Vanovschi, V.; Vogt, L.; Vydrov, O.; Wang, T.; Watson, M. A.; Wenzel, J.; White,

A.; Williams, C. F.; Yang, J.; Yeganeh, S.; Yost, S. R.; You, Z.-Q.; Zhang, I. Y.; Zhang, X.; Zhao, Y.; Brooks, B. R.; Chan, G. K. L.; Chipman, D. M.; Cramer, C. J.; III, W. A. G.; Gordon, M. S.; Hehre, W. J.; Klamt, A.; III, H. F. S.; Schmidt, M. W.; Sherrill, C. D.; Truhlar, D. G.; Warshel, A.; Xu, X.; Aspuru-Guzik, A.; Baer, R.; Bell, A. T.; Besley, N. A.; Chai, J.-D.; Dreuw, A.; Dunietz, B. D.; Furlani, T. R.; Gwaltney, S. R.; Hsu, C.-P.; Jung, Y.; Kong, J.; Lambrecht, D. S.; Liang, W.; Ochsenfeld, C.; Rassolov, V. A.; Slipchenko, L. V; Subotnik, J. E.; Voorhis, T. Van; Herbert, J. M.; Krylov, A. I.; Gill, P. M. W.; Head-Gordon, M. *Mol. Phys.* **2015**, *113*, 184–215.

(34) Tang, M. L.; Reichardt, A. D.; Wei, P.; Bao, Z. *J. Am. Chem. Soc.* **2009**, *131*, 5264–5273.

(35) Subhas, A. V; Whealdon, J.; Schrier, J. *Comput. Theor. Chem.* **2011**, *966*, 70–74.

(36) Gruhn, N. E.; Filho, D. A. da S.; Bill, T. G.; Malagoli, M.; Veaceslav Coropceanu; Antoine Kahn; Brédas, J.-L. *J. Am. Chem. Soc.* **2002**, *124*, 7918–7919.

(37) Kato, T.; Yamabe, T. *J. Chem. Phys.* **2001**, *115*, 8592–8602.

(38) Salman, S.; Delgado, M. C. R.; Coropceanu, V.; Brédas, J.-L. *Chem. Mater.* **2009**, *21*, 3593–3601.

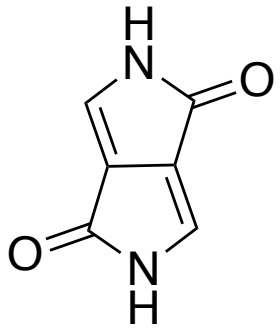

347

348 **Figure 1**. The diketopyrrolopyrrole (DPP) unit.

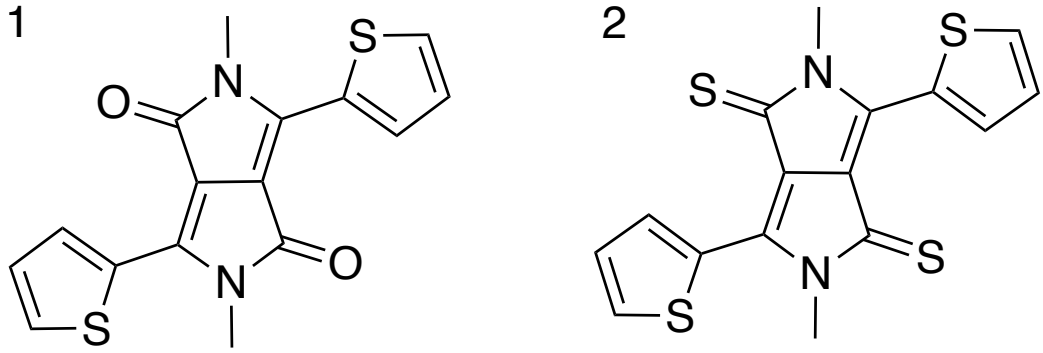

349

350 **Figure 2.** Diketopyrrolopyrrole-dithienyl (**1**) and dithiopyrrolopyrrole-dithienyl (**2**).

351

352

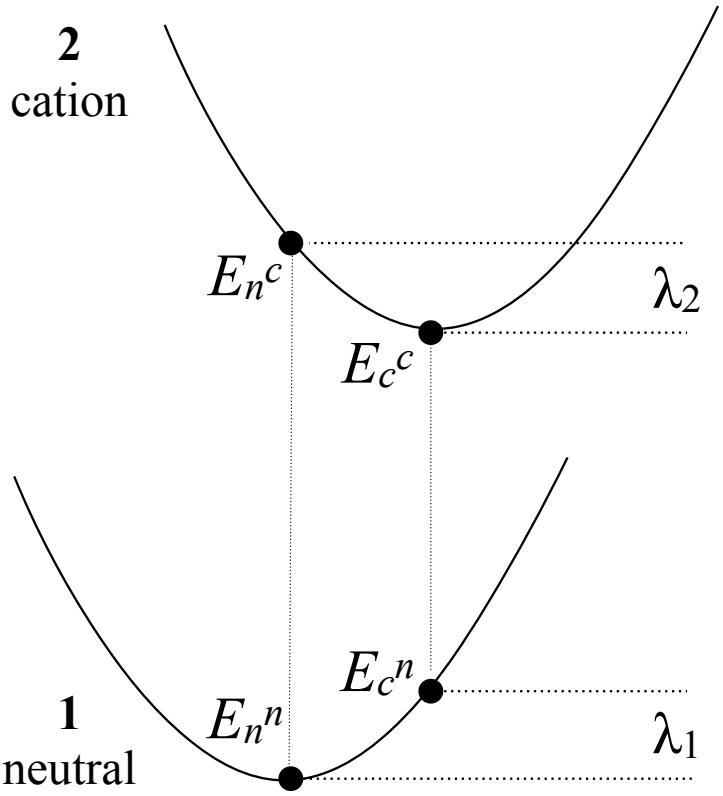

353
354 **Figure 3.** The calculation of the RE from the adiabatic potential energy surfaces of the
355 cation and neutral states as $\lambda_+ = \lambda_1^+ + \lambda_2^+ = E_c^n - E_n^n + E_n^c - E_c^c$. The subscript refers to
356 the optimized geometry and the superscript refers to the charge state, i.e. E_c^n is the total
357 electronic energy of the neutral molecule at the optimized cation geometry. The total RE
358 for the hole transfer is calculated as $\lambda_+ = \lambda_1^+ + \lambda_2^+$. In the rest of this article, we refer to
359 the RE as λ_+ and λ_- for the hole- and electron transfer processes, respectively.

360

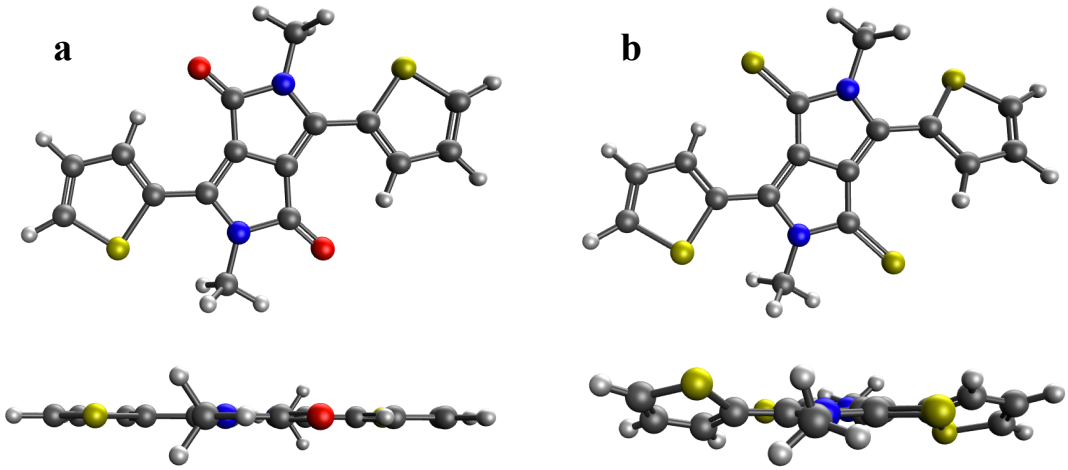

361
362 **Figure 4.** The top and side view of the optimized geometries for molecules **1** (a) and **2** (b).

363

364 **a**

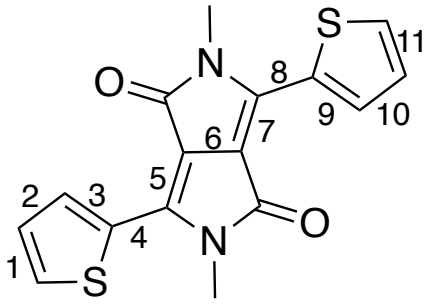

365

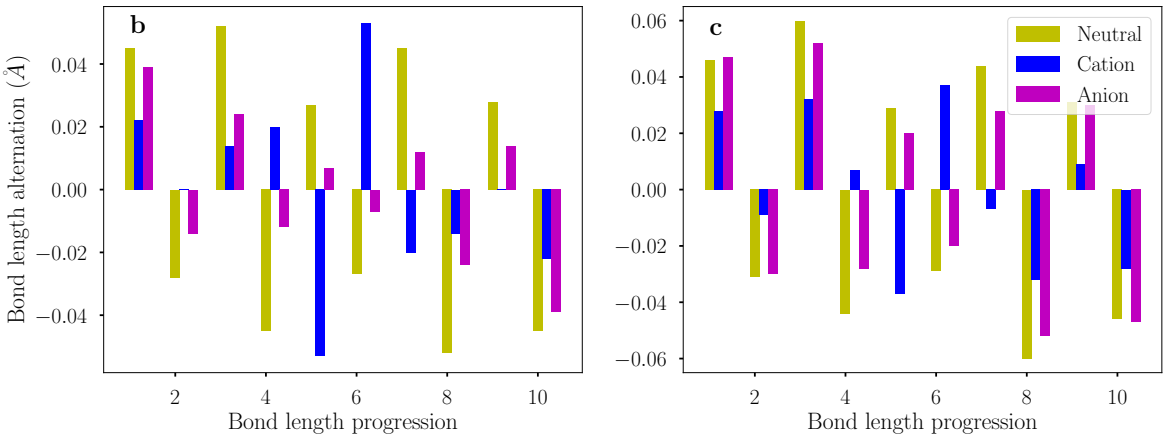

366

367 **Figure 5**. Bond length alternation of molecules **1** (b) and **2** (c) for the conjugation pathway

368 as labeled in (a).

369

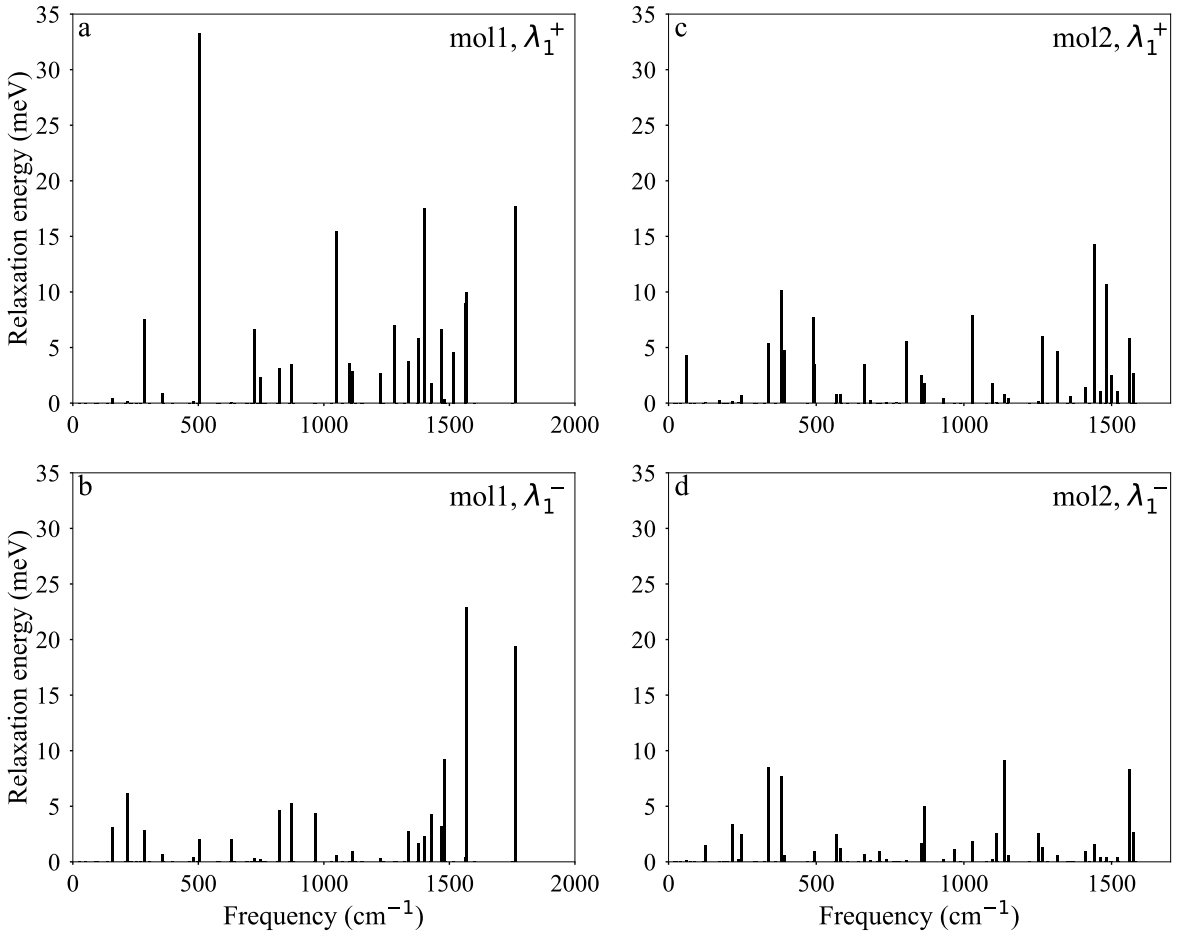

Figure 6. Contributions of the vibrational modes to the hole- and electron relaxation energy in molecule **1** and **2**

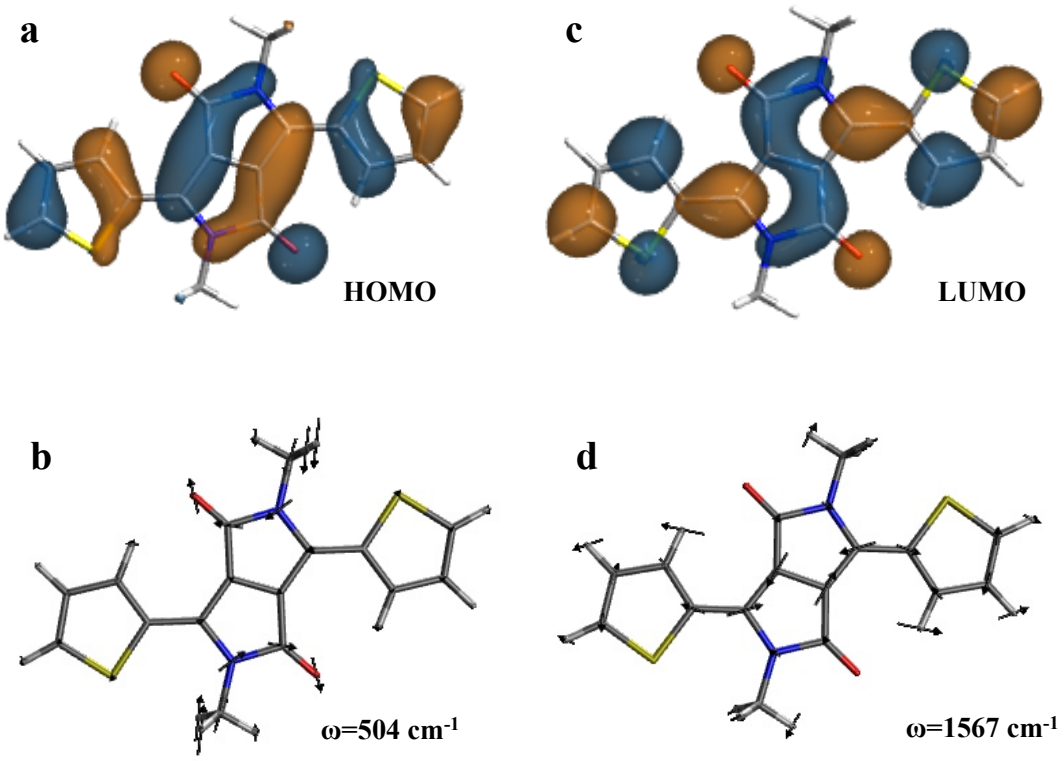

374

375 **Figure 7.** The HOMO (a) and LUMO (c) wavefunctions and the normal modes with strong

376 hole (b) and electron (d) vibronic coupling in molecule **1**.

377

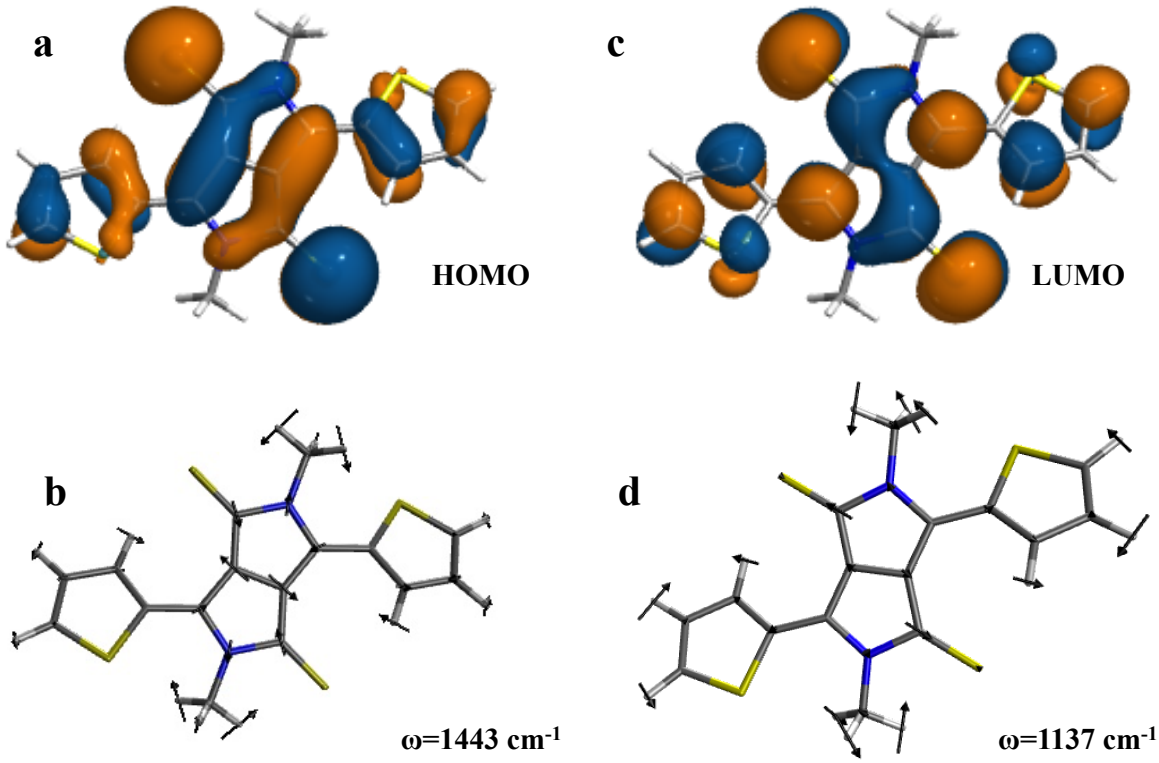

Figure 8. The HOMO (a) and LUMO (c) wavefunctions and the normal modes with strong hole (b) and electron (d) vibronic coupling in molecule **2**.

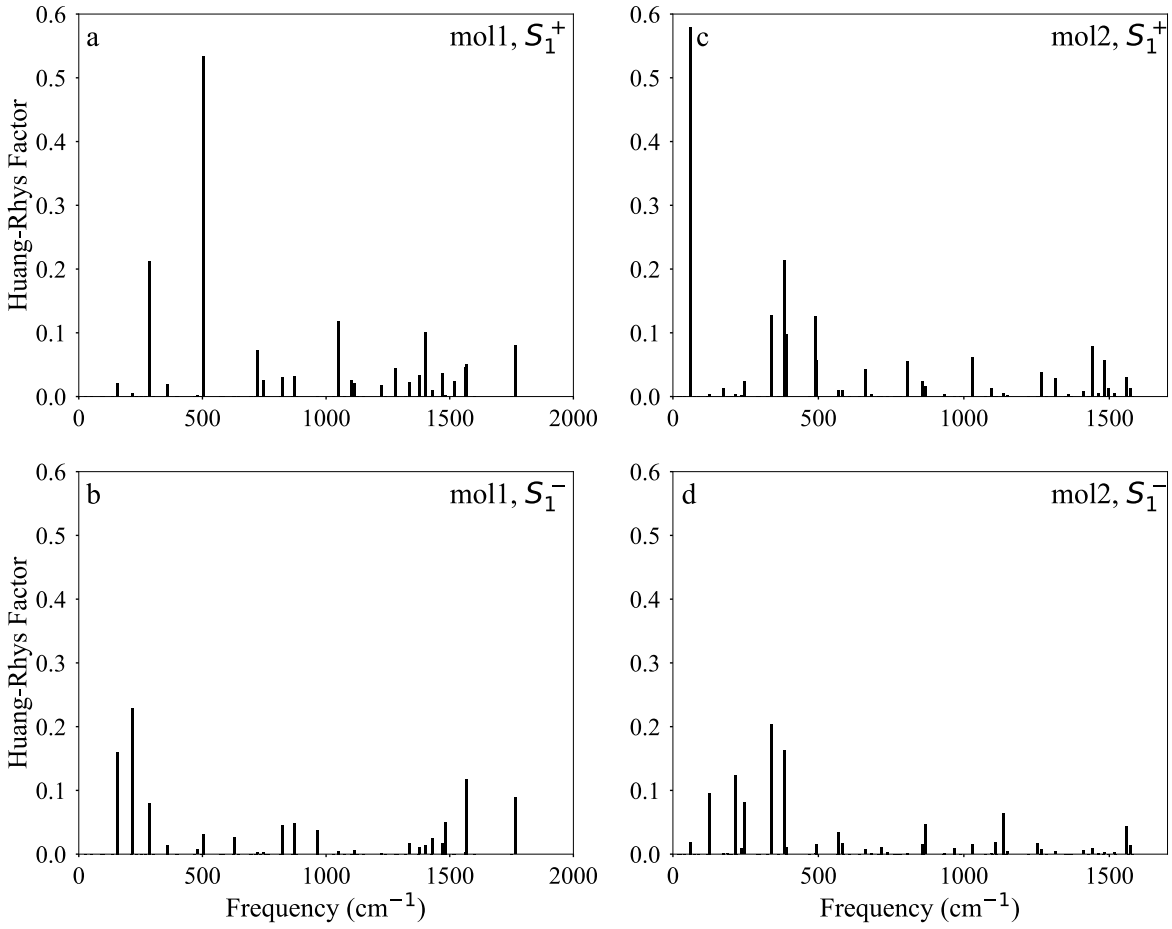

Figure 9 Huang-Rhys factors for the vibrational modes in the hole- and electron relaxation in molecule **1** and **2**

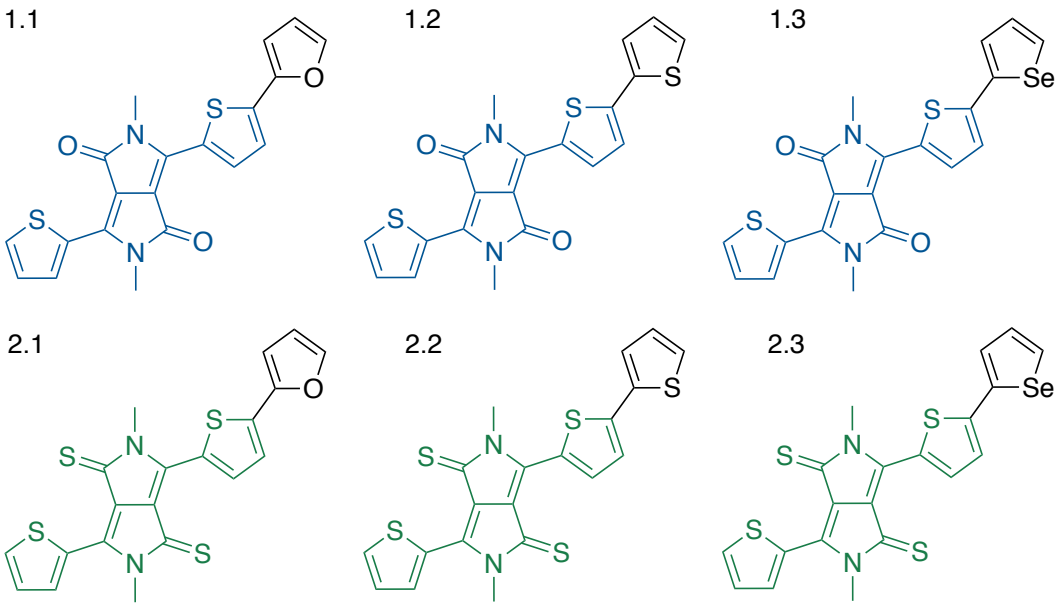

386

387 **Figure 10** The oligomers derived from molecule **1** and **2**.

388

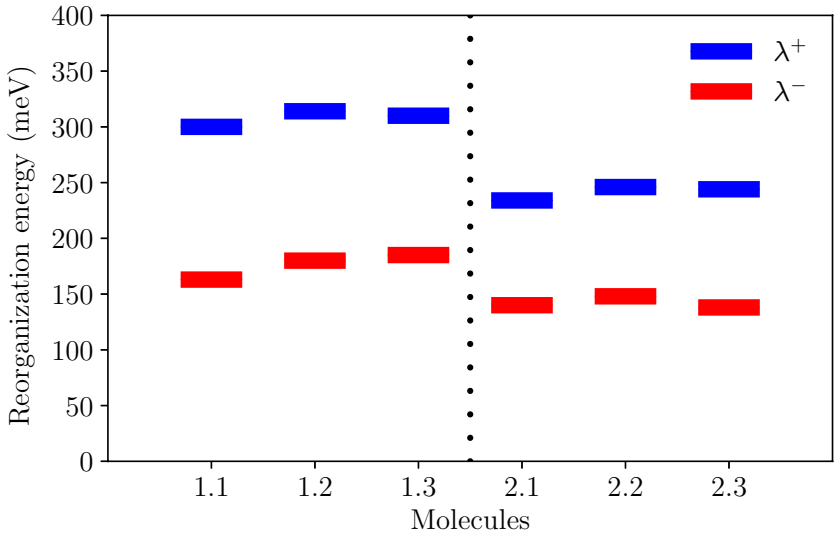

Figure 11 The reorganization energy values for the oligomers shown in Figure 10. The dotted line separates molecule **1** and **2** derived units.

Table 1. Frontier orbital energy level values, electron affinity (EA), ionization potentials (IP) and the total reorganization energies from the adiabatic surfaces (λ) and normal mode analysis (λ^{nm}) for the hole and electron transfer for molecule **1** and **2**.

Mol	ϵ_{homo}	ϵ_{lumo}	ϵ^{c}_{homo}	IP_{adia}	EA_{adia}	λ^{+}	λ^{-}	λ^{+nm}	λ^{-nm}
1	-4.980	-2.530	-4.653	6.239	2.413	331	196	333	196
2	-5.142	-3.020	-4.925	6.396	2.658	217	141	220	142

All values are in eV, except λ which are in meV**.**

Table 2. Huang-Rhys factors (unitless) and the decomposition of the RE over the vibrational frequencies of molecule **1**.

No	ω (cm^{-1})	S_1^+	S_1^-	λ_1^+(meV)	λ_1^-(meV)
7	**158**	0.021	0.160	0.415	3.138
10	**218**	0.006	0.229	0.156	6.178
16	**285**	0.213	0.080	7.514	2.833
18	**358**	0.020	0.015	0.889	0.647
23	**479**	0.003	0.007	0.181	0.425
25	**504**	0.533	0.032	33.304	1.985
29	**631**	0.000	0.026	0.035	2.058
35	**723**	0.074	0.003	6.596	0.277
37	**746**	0.025	0.002	2.356	0.214
41	**823**	0.031	0.046	3.151	4.675
43	**871**	0.032	0.048	3.455	5.22
49	**967**	0.000	0.037	0.000	4.396
51	**1052**	0.118	0.005	15.44	0.620
53	**1101**	0.026	0.000	3.539	0.021
55	**1114**	0.020	0.007	2.829	0.900
59	**1225**	0.018	0.002	2.700	0.309
61	**1281**	0.044	0.000	7.000	0.006
64	**1337**	0.023	0.016	3.754	2.724
66	**1376**	0.034	0.010	5.784	1.703
67	**1401**	0.101	0.013	17.506	2.268
69	**1429**	0.110	0.024	1.754	4.313
70	**1470**	0.036	0.017	6.588	3.163
72	**1482**	0.002	0.050	0.326	9.190
76	**1518**	0.024	0.000	4.520	0.021
78	**1564**	0.046	0.002	8.982	0.406
80	**1567**	0.051	0.118	9.978	22.933
83	**1764**	0.081	0.089	17.677	19.362

404 **Table 3.** Huang-Rhys factors (unitless) and the decomposition of the RE over the

405 vibrational frequencies of molecule **2**.

No	ω (cm^{-1})	S_1^+	S_1^-	λ_1^+(meV)	λ_1^-(meV)
2	**41**	0.001	0.000	0.007	0.00
3	**60**	0.579	0.019	4.316	0.141
7	**126**	0.003	0.096	0.053	1.502
8	**173**	0.013	0.002	0.277	0.044
12	**217**	0.005	0.124	0.124	3.336
14	**236**	0.002	0.009	0.071	0.25
15	**245**	0.024	0.082	0.737	2.479
19	**339**	0.128	0.203	5.378	8.534
21	**384**	0.214	0.162	10.16	7.713
22	**391**	0.098	0.011	4.732	0.545
24	**491**	0.126	0.001	7.687	0.071
25	**493**	0.057	0.016	3.461	0.963
27	**569**	0.011	0.035	0.767	2.465
28	**584**	0.011	0.017	0.794	1.245
32	**662**	0.043	0.008	3.519	0.634
33	**684**	0.003	0.002	0.282	0.135
35	**716**	0.000	0.011	0.014	0.947
37	**737**	0.000	0.002	0.027	0.219
42	**805**	0.055	0.002	5.510	0.179
44	**857**	0.024	0.016	2.522	1.686
46	**867**	0.016	0.046	1.762	4.995
48	**932**	0.004	0.002	0.420	0.204
49	**967**	0.000	0.010	0.004	1.152
51	**1030**	0.062	0.015	7.920	1.878
53	**1096**	0.013	0.001	1.802	0.188
55	**1110**	0.000	0.018	0.025	2.523
57	**1137**	0.005	0.064	0.768	9.092
59	**1151**	0.003	0.004	0.395	0.577
61	**1252**	0.001	0.016	0.193	2.534
63	**1267**	0.038	0.008	6.043	1.305
65	**1316**	0.028	0.004	4.615	0.617
67	**1360**	0.004	0.000	0.626	0.000
69	**1412**	0.008	0.006	1.434	0.987
71	**1443**	0.080	0.009	14.284	1.569
73	**1464**	0.006	0.002	1.069	0.365
75	**1484**	0.058	0.002	10.64	0.387

77	**1499**	0.014	0.000	2.509	0.032
78	**1519**	0.006	0.002	1.081	0.441
80	**1560**	0.030	0.043	5.786	8.289
82	**1573**	0.014	0.013	2.701	2.614

406

407

Table 4. Frontier orbital energy level values, electron affinity (EA), ionization potentials (IP) and the total reorganization energies from the adiabatic surfaces (λ) for the hole (+) and electron (-) transfer for the molecules in Figure 10.

Molecule	ϵ_{homo}	ϵ_{lumo}	IP_{adia}	EA_{adia}	λ^{+}	λ^{-}
1.1	-4.834	-2.565	5.957	1.406	300	163
1.2	-4.873	-2.606	5.978	1.480	314	180
1.3	-4.875	-2.625	5.975	1.512	310	185
2.1	-5.020	-2.995	6.136	1.855	234	140
2.2	-5.047	-3.027	6.150	1.663	246	148
2.3	-5.054	-3.057	6.120	1.497	244	138

All values are in eV, except λ, which are in meV**.**